1

Intelligent Reflecting Surfaces Assisted Hyperloop Wireless Communication Network

Wafa Hedhly, Osama Amin, Mohamed-Slim Alouini, and Basem Shihada

Abstract—Hyperloop or evacuated-tube transportation is a groundbreaking technology that can reach aircraft-like speeds. Its uncommon configuration of a steel-made tube isolates the moving pod from the outside wireless world. In this work, we propose an inner tube network architecture that can provide the moving pod with a seamless and reliable connection. The proposed network consists of successive access points (APs) and intelligent reflecting surfaces (IRS) strategically positioned along the tube and connected to a control station (CS) through wired links to improve the wireless cell coverage. The subsequent entities of the proposed design are intelligently placed along the movement path, steering the transmitted beam towards the receiver, while a soft handover is achieved between consecutive cells. First, we optimize each IRS's positioning and phase shifts to maximize cell coverage thanks to the IRS scanning abilities while keeping a minimum quality of service. Afterward, we exploit the centralized operation at the CS and design a soft handover scheme for the inner-tube wireless network. The numerical results show that the proposed approach provides good cell coverage and spectral efficiency with different IRS scanning ranges.

Index Terms—Hyperloop communications, vacuum tube communications, high-speed flying train, vactrain, intelligent reflecting surfaces, reconfigurable intelligent surfaces, metasurface, beam steering.

1 Introduction

THE flying train concept is shaping up, enabling super-**_** sonic speed transportation. Hyperloop is a novel solution that breeds immense advantages for people and freight transportation. The overall design aims to reach speeds of over 1000 km/h by integrating magnetic levitation and propulsion in a pressurized environment [1], [2]. The Hyperloop system exhibits a complex structure, incorporating various technologies to move at tremendous speeds. Under these exceptional circumstances and unique scenarios, the employed communication system should provide reliable connectivity under several challenges. The adopted sealed steel-structured tube in the Hyperloop prevents signal penetration, isolating the inner world from the outside and creating a highly scattering environment for electromagnetic (EM) waves. Also, the exceptionally high speed of the traveling pod results in severe Doppler shifts and frequent handovers, leading to increased transmission errors and delays. In addition, applying conventional high-speed rail wireless communication solutions to Hyperloop hits a bottleneck because of the high-speed traveling pod and the lack of appropriate channel models and system designs [3].

Intelligent reflecting surfaces (IRSs) or reconfigurable intelligent surfaces are being recognized as a revolutionary technology that provides a new perspective on future wireless systems and addresses several design challenges through the generalization of the conventional laws of EM waves [4]. IRSs offer a new degree of freedom, with a wide variety of functionalities allowing wavefront manipulation via an ultrathin and compact structure [5]. An IRS-based system can achieve fast and efficient beamsteering, which supports tracking-based systems with a good accuracy [6]—

The authors are with the Computer, Electrical and Mathematical Sciences and Engineering (CEMSE) Divison, King Abdullah University of Science and Technology (KAUST), Thuwal 23955, Makkah Prov., Saudi Arabia (e-mail: {wafa.hedhly, osama.amin, slim.alouini, basem.shihada}@kaust.edu.sa).

[8]. Different from the conventional beam-steering approach achieved through phased array antennas and digital beamforming, the IRS-based steering system cope with the limitations of the conventional systems. Specifically, the IRSbased system is less expensive than the phased-array antenna system [9] as the latter requires a high number of phase shifters with their control circuitry along with the feeding network that is very complex [6]. On the other hand, digital beamforming systems need a separate RF chain per antenna element [10], [11]. Hence, the IRS-based system can provide a promising simple structure beamsteering solution that can achieve high beamforming gain, similar to massive MIMO but with a reduced energy and hardware cost [12]. Along this line, the performance of wireless systems can be optimized through the design of the IRS passive beamforming through an adaptive tuning of the phase-shifts. The objective varies between maximizing rate performance [13], reducing power consumption [14], or proposing energyefficient schemes [15]. In order to reduce channel state information (CSI) overhead, a novel scheme based on the illumination of the mobile user within a certain area was proposed in [16].

Traditional communication systems face significant challenges when deployed inside tubes for high-speed pod communication. For example, bouncing signals and multipath interference can degrade link performance. Moreover, the tube's small radius (around 2 m) results in limited transmission ranges of wireless signals. Hence, a customized solution is needed for Hyperloop communication to address these challenges. We propose a novel architecture for the Hyperloop downlink communication network using IRS beamsteering. The system exploits the IRS's tuning capabilities and antenna/IRS configuration to mitigate the harsh tube environment. The IRS reflects and steers signals towards moving pods. Their compact profile and recon-

figurability suit the tight tube space. Our proposed IRS-based solution avoids multipath interference and improves performance. It directs a focused beam at the pod receiver, effectively avoiding reflected signals. The contributions are summarized as follows:

- We propose a system architecture that can avoid the multipath, overcome Doppler effect and improve the cell coverage of the communication network insider the limited space inner-tube. The system comprises successive APs mounted on the tube wall, each with a highly directed transmit antenna radiating towards its corresponding IRS. The antenna transmits a narrow beam to avoid interference from reflections inside the tube and increase the coverage of each AP. Hence, it is necessary to address this limitation to reduce the implementation cost of Hyperloop communication network. A promising solution is to track the receiver using automatic adjustment of the IRS phase shifts while avoiding multipath and compensating for the Doppler effect.
- We tune the IRS positioning parameters to increase cell coverage for the network inside the tube while keeping a minimum quality of service. The system employs millimeter wave technology because lower frequency technologies require bulky components, which is inconvenient for the limited space of the tube. Moreover, lower-frequency signals have wide beam angles leading to increased scattering events and reduced transmission ranges. We formulate and solve the corresponding optimization problem with the objective of cell coverage maximization while maintaining a minimum DL data rate.
- We design the multi-cell configuration considering a soft handover between successive wireless cells to ensure a smooth transition with reliable communication links quality. We tune the overlap distance between successive cells to minimize the system handover rate while maintaining a minimum DL data rate. The simulation-based evaluation considers realistic parameters for the tube and pod dimensions based on HyperloopTT technology prototype [17].

The rest of the paper is organized as follows. Section II provides a detailed description of the proposed system and the benefit of using an IRS. In section III, we present the IRS parameters and system model. Section IV provides the single-cell design that can maximize cell coverage. Then, section V offers the multi-cell design based on a minimum overlap area between successive cells to ensure handover execution. In section VI, we provide the simulation results. Finally, we conclude the work in section VII.

2 RELATED WORK

Recently, Hyperloop communication started drawing the attention of the vehicular communication research community to cope with its particular communication requirements. The related research investigated appropriate system solutions to address the associated unique challenges, where the research directions covered antenna designs [18]–[20], channel modeling [21], [22] and network architectures [20],

[23]-[25]. Several attempts focused on characterizing the channel inside the tube using deterministic approaches [21], [22]. However, real-field measurements are still required to validate and adjust the proposed model in order to consider it for the communication system design. Regarding the network architectures design, Han et al. adopted a distributed base-stations wireless network to reduce handover failure by creating redundant remote radio and baseband units [23]. On the other hand, a centralized cooperative cloud radio access network is utilized to address the frequent handover using the moving-cell scheme and optical switching with a primary focus on tube-to-ground communications [20], [24], [25]. The objective was to benefit from the moving-cell scheme to lower the frequency of connections/disconnections when moving between successive cells. Although the moving-cell approach has promising merits in addressing frequent handoffs in high-speed scenarios, it is still an evolving technology and not mature enough to be implemented in real-life systems. Also, it imposes higher cost and complexity on both the APs inside the tube and the network controlling stations [26]. So far, the available research efforts lack in-depth analysis and simulations, which are insufficient to address the peculiarities and strict requirements of Hyperloop communications. Thorough justifications of the system's choices are necessary to ensure a robust communication system. Interestingly, dealing with the peculiarities of the Hyperloop environment can be achieved through intelligent technologies and innovative solutions. Herein, we utilize smart surfaces to propose and evaluate a downlink (DL) inner-tube network solution capable of overcoming the harsh communication environment inside the tube.

3 IRS-ASSISTED WIRELESS SYSTEM FOR INNER-TUBE COMMUNICATIONS

This section proposes an adaptive IRS-based wireless communication system suitable for the Hyperloop inner tube architecture. The system consists of successive transmitters, or APs mounted on the tube's ceiling and connected to a control station (CS) through an optical fiber that works as a backhaul link, as shown in Fig. 1. The CS can execute complex, expensive signal processing algorithms to minimize the operations conducted at each AP. The tube is divided

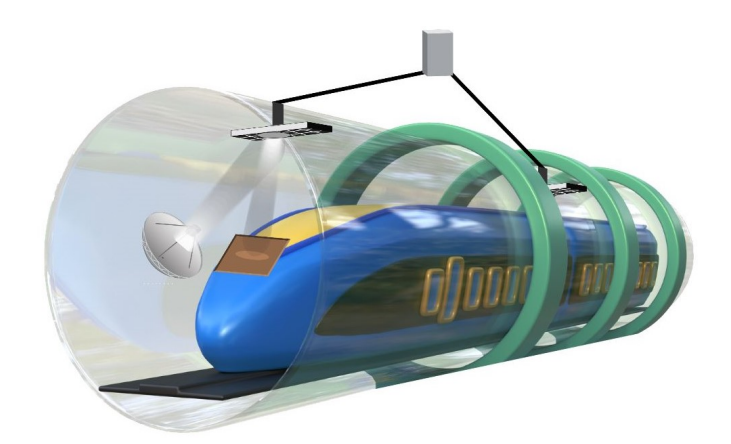


Figure 1: Inner-tube wireless network.

into successive sections/cells along its axis, where each cell is covered by at least one AP, as depicted in Fig. 1. Each transmitter is composed of an optical-to-electrical converter, a single highly directive transmit antenna, and an IRS to steer the beam towards the receiver mounted on the top of the moving pod, which acts as a mobile relay (MR). All user equipment (UE) inside the pod connects with the MR to communicate with the core network. The directive transmit antenna mounted on the tube can generate a pencil beam directed towards the IRS mounted on the ceiling, as shown in Fig. 2. These positions guarantee visibility, i.e., a direct link between each antenna and its corresponding IRS.

The proposed configuration operation is managed centrally by the CS to guarantee fast execution times. Prompt decisions and efficient traffic management are crucial for the Hyperloop system performance to handle the datahungry services considering the pod's speed that results in frequent handovers. Therefore, the network inside the tube comprises successive partially overlapped wireless cells to ensure a smooth transition between the cells. We first describe the intracell and intercell configurations before modeling the Hyperloop system and designing the related parameters.

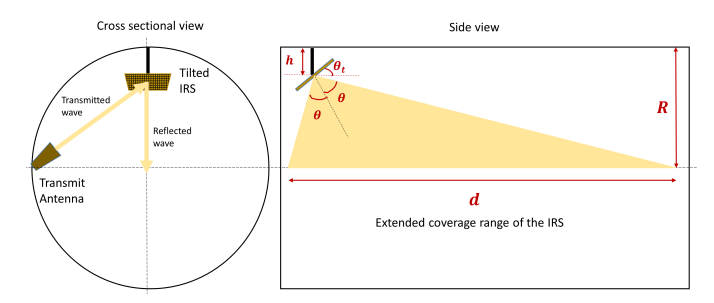


Figure 2: Proposed system setup.

3.1 Intracell System Configuration

The IRS angle range determines the cell coverage along the tube axis. We consider symmetric IRS, i.e., the beam scanning is between $-\theta$ and $+\theta$, $\theta \in [0,\pi/2]$ allowing a horizontal coverage distance of d m in a tube with a cross-section radius of R m. The IRS scans the cell with a specific switching time to track the pod movement with a speed of v m/s. To meet the cell coverage limitations due to limited IRS scanning range, we place the IRS in a tilting position with angle θ_t below the tube wall by h m, as depicted in Fig. 2. The proposed configuration extends the distances range of each cell from $d=2R\tan(\theta)$ to

$$d = (R - h) \left(\frac{1}{\cos^2(\theta - \theta_t)} + \frac{1}{\cos^2(\theta + \theta_t)} - \frac{2\cos(2\theta)}{\cos(\theta - \theta_t)\cos(\theta + \theta_t)} \right)^{\frac{1}{2}}.$$

The cellular coverage range depends on the constrained scanned angular range. For example, when the maximum IRS scanning angle is $\theta=\pm50^\circ$ and $R=1.75\,\mathrm{m}$, then, the cellular coverage range is $d=4.17\,\mathrm{m}$. However, with our proposed setup depicted in Fig. 2, we can overcome the distance limitations and increase the coverage of each cell. For instance, if $\theta_{\rm t}=39^\circ$ and $h=5\,\mathrm{cm}$, the range increases to $d=97.72\,\mathrm{m}$; as can be computed from (1). It is worth noting

that we impose $\theta+\theta_{\rm t}<\pi/2$ to avoid the IRS radiating towards the ceiling and creating undesirable reflections. Hence, the parameters $\theta_{\rm t}$ and h introduce two extra degrees of freedom to the design, which can relax the IRS scanning requirements. According to the distance expression in (1), the radius of the tube R contributes to the limited transmission ranges inside the tube. Fortunately, the cell coverage depends also on the IRS positioning parameters, providing further variables to adjust the distance, which helps mitigate the tube space limitation. It is important to mention that the proposed tilting position is particularly convenient with IRSs because they are thin, simple structures requiring limited space, with no RF chains or bulky components.

The receiver arrival angle varies with the distance between the IRS and the receiver, which changes with the pod movement. Although omnidirectional antennas can avoid connection disruption, they have low gain, limiting data rates-hungry services. Hence, we opt to use a multi-sector planar antenna operating at the millimeter-wave band to cope with visibility and data rate requirements. For example, a multi-sector antenna can divide the radiation pattern into eight sectors covering 22.5°, allowing it to cover 180° over the azimuth plane and 66° over the elevation plane with a possible gain per sector of 13 dBi [27], as depicted in Fig. 3. Hence, the multi-sector planar antenna is promising for this specific system setup. In order to prevent the deterioration of the communication signal-to-noise ratio (SNR), we consider that a partial area of the receiving antenna surface is illuminated by the IRS. Therefore, multipath components are avoided because the transmitted signal is entirely captured by the receiving antenna.

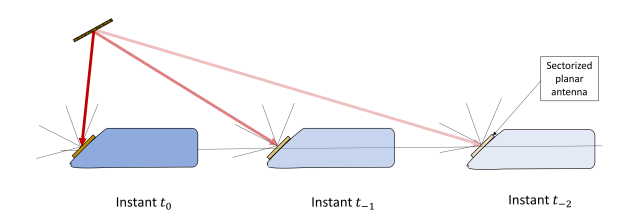


Figure 3: Multi-sector antenna at the receiver.

The temporal transmission scheme of the proposed system adopts a burst transmission, where high-bandwidth signals are transmitted over short periods. Such a transmission scheme is necessary due to the interruption caused by the switching time dedicated for the IRS phase shift adjustment according to the pod's position, as illustrated in Fig. 4. The parameters t_{Data} and τ_{switch} are the two-time intervals characterizing the transmission over time, which represent the data downloading interval and the silence interval dedicated for the IRS switching process, respectively. Since the pod is in constant motion, t_{Data} depends on the time during which visibility between the transmitter and receiver is guaranteed, which we call $t_{\rm vis}$. Several parameters control $t_{
m vis}$ such as the antenna size and profile area. To avoid packets loss caused by beam misalignment, we use $t_{\mathrm{Data}} < t_{\mathrm{vis}}$, which allows downloading data for $\eta = \frac{t_{\mathrm{Data}}}{t_{\mathrm{Data}} + r_{\mathrm{switch}}}$ of the total time.

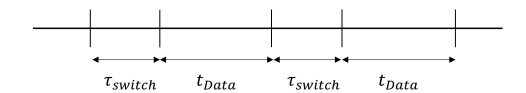


Figure 4: System behavior in time.

3.2 Intercell System Configuration

The considered system architecture adopts group handover, where all UEs inside the pod connect to an MR in the pod, in order to alleviate the handover process and reduce the probability of handover failure and dropped connections. The group handover system is illustrated in Fig. 5.

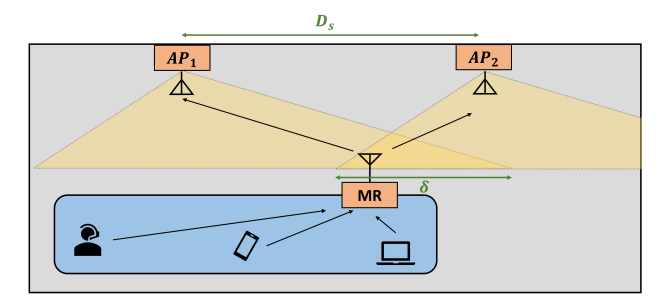


Figure 5: Group handover.

The movement pattern of the Hyperloop pod is deterministic, unlike most general dynamic scenarios where the movement direction, velocity, and other factors are random variables [28]. Hence, the CS has prior knowledge of the exact instantaneous location of the pod due to its predefined velocity and movement trajectory inside the tube. Therefore, we employ a soft handover process during the intercell movement, where the receiver maintains its connection with the serving cell while establishing a new connection with the target cell. The transmission is transferred from an AP to the next one in the overlap area between adjacent cells according to the received SNR to avoid connection disruption during the travel journey.

Since frequent handovers are one of the major challenges for Hyperloop, the proposed multi-cell system design is established based on the handover rate $H_{\rm r}$ performance metric, which is defined as in [28], as the number of handover per unit time,

$$H_{\rm r} = \frac{\text{Number of handovers}}{\text{Journey Duration}}.$$
 (2)

If we consider $D_{\rm T}$ the total length of the tube and $N_{\rm c}$ the number of cells, the journey (travel) duration is equal to $D_{\rm T}/v$. Thus, $H_{\rm r}$ reduces to

$$H_{\rm r} = \frac{N_{\rm c} - 1}{D_{\rm T}} v. \tag{3}$$

If we denote the separation distance between two successive APs by $D_{\rm s}$, and the overlap distance between successive cells by δ , we can prove that $N_{\rm c}$ satisfies the following equation 1 ,

$$N_{\rm c} - 1 = \frac{D_{\rm T} - d}{d - \delta}.\tag{4}$$

1. where $d = \delta + D_s$ and the total distance $D_T = (N_c - 1)D_s + d$.

Hence, the handover rate can be written as,

$$H_{\rm r} = \frac{D_{\rm T} - d}{(d - \delta)D_{\rm T}}v. \tag{5}$$

Undesirable communication interruptions and signaling overhead occur when the handover rate increases, leading to a reduced throughput [29]. Although the very high speed of the pod drastically increases the handover rate, signaling overhead is less influential in the case of Hyperloop communications because of prior knowledge of the pod's location, speed, and movement direction. The CS efficiently exploits this information to simplify the handover procedure, which is initiated at the CS before reaching the overlap area between two cells.

4 SYSTEM MODELING

In this section, we present the mathematical model of the proposed Hyperloop system to characterize the IRS operation, followed by the proposed system configuration and ending with the achievable rate as the adopted performance metric.

4.1 Intelligent reflecting surface characteristics

The general IRS concept is based on introducing phase discontinuities along its surface, which results in a modified or anomalous angle of reflection. Hence, we can create a desired phase gradient over the IRS surface by configuring individual elements. The transmitted wave undergoes a phase shift adjustment for each element to create the desired field distribution. Hence, we need to find the appropriate reflection coefficient that steers the signal towards the receiver. The whole operation is mainly based on Snell's Generalized law of reflection. Figure 6 depicts an example of the IRS reflection process, where the surface is discretized into subwavelength elements, each with a constant phase shift to realize a target phase gradient.

The adopted IRS consists of an $N \times M$ planar array of electrically controllable identical unit cells U_{nm} , $1 \le n \le N$ and $1 \leq m \leq M$ each with dimensions a and b that are in the order of sub- λ $\left[\frac{\lambda}{10},\frac{\lambda}{2}\right]$ [30]. The whole operation is mainly based on Snell's Generalized law of reflection in terms of the IRS phase gradient $d\Phi/dx$ along the x-axis, where the relationship between the angle of incidence θ_i and angle of reflection $\theta_{\rm r}$ is expressed in terms of a specific wavelength λ and a medium refractive index n_i as $\sin{(\theta_{\rm r})} - \sin{(\theta_{\rm i})} = \frac{\lambda}{2\pi n_{\rm i}} \frac{d\Phi}{dx}$ [31]. The reflection coefficient of U_{nm} is denoted by $\Gamma_{nm} = A_{nm}e^{j\phi_{nm}}$, where A_{nm} is the amplitude of the reflection coefficient, $A_{nm} < 1$ and ϕ_{nm} is the phase shift introduced by the unit cell, $0 \le \phi_{nm} < 2\pi$. Here, we assume that the IRS does not affect the amplitude of the reflected signal, i.e., $A_{nm} = |\Gamma_{nm}| = 1$. The phase ϕ_{nm} can be controlled through the IRS controller to shape the scattered field and therefore focus the reflected beam towards the direction of the receiver.

The propagation model when using controllable metasurfaces is different from traditional scenarios, where it involves additional parameters characterizing the IRS, such

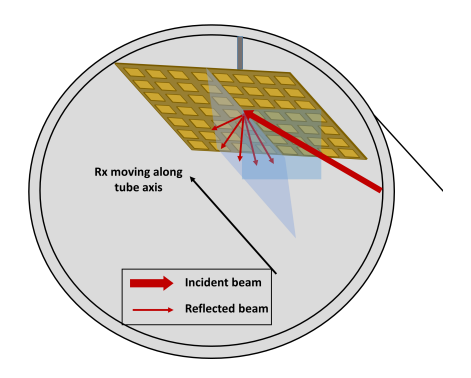


Figure 6: IRS reflection process.

as the phase shifts. According to [32], [33], the pathloss between the Tx and Rx, through a single unit cell, is expressed as follows,

$$\alpha = \frac{G_{\rm t}G_{\rm r}}{(4\pi)^2} \left(\frac{ab}{d_{\rm s}d_{\rm r}}\right)^2 \cos^2(\theta_{\rm i}) \cos^2(\theta_{\rm r}),\tag{6}$$

where $G_{\rm t}$ and $G_{\rm r}$ are the antenna gain of the transmitter and receiver, respectively, $d_{\rm r}$ is the distance between the Rx and the IRS and $d_{\rm s}$ is the distance between the Tx and IRS. We consider a linearly polarized incident wave. The general model can be found in [34].

4.2 System Model

We consider a DL IRS-assisted wireless communication system where both Tx and Rx are equipped with an antenna, with respective gains of $G_{\rm t}$ and $G_{\rm r}$. We assume a highly-directive pencil beam transmit antenna to beat the rich scattering environment inside the sealed tube. On the other side, the multi-sector receive antenna has a wide reception area to avoid beam misalignment between the Tx and Rx. The Tx antenna directs the transmitted beam towards the IRS placed on the tube. Then, the IRS reconfigures the transmission angle of the beam and steers the reflected signal towards the moving Rx. Hence, the transmit antenna and the IRS form an efficient and less complex beam steering system.

The deterministic channel enabled by a closed environment and known pod path allows pre-configuring the IRS with the analytically computed path loss, focusing beams toward the receiver pod. With fast reconfigurability of IRS materials, the IRS system can track the pod receiver despite its high speed.

In this setup, the AP is the source connecting the pod to the network, while the IRS is a reflector that tracks the moving pod. This proposed setup is a suitable solution to establish a reliable and stable wireless link in the line-of-sight (LoS) direction. The adjustment of the IRS pattern to achieve the desired beam direction is performed by a controller connected to the IRS. The receiver is assumed to be moving in the z-direction as the axis of the tube. For simpler notations, we consider the IRS elements arranged from 1 to NM. Then, instead of using U_{nm} , $1 \le n \le N$, $1 \le m \le M$, we use the notation U_ℓ , where $1 \le \ell \le NM$. Thus, the received signal is expressed as [32],

$$y = \sqrt{\alpha} \, \mathbf{h}_{\mathbf{s}}^{\mathbf{H}} \, \mathbf{\Phi} \, \mathbf{h}_{\mathbf{r}} x + w, \tag{7}$$

where $\mathbf{h}_{\mathrm{s}} = [e^{j\psi_{\mathrm{n}}^{\mathrm{s}}}, \ldots, e^{j\psi_{\mathrm{n}}^{\mathrm{s}}}, \ldots, e^{j\psi_{NM}^{\mathrm{s}}}]^{\mathrm{T}}$ represents the phase shifts of the LoS channels between the source and IRS elements, $\mathbf{h}_{\mathrm{r}} = [e^{j\psi_{\mathrm{1}}^{\mathrm{r}}}, \ldots, e^{j\psi_{\mathrm{n}}^{\mathrm{r}}}, \ldots, e^{j\psi_{NM}^{\mathrm{r}}}]^{\mathrm{T}}$ represents the phase shifts of LoS channels between the IRS elements and receiver, $\mathbf{\Phi} = \mathrm{diag}(e^{j\phi_{1}}, \ldots, e^{j\phi_{n}}, \ldots, e^{j\phi_{NM}})$ is a diagonal matrix representing the phases added by each surface element, x is the transmitted signal with power p_{t} and w is an additive white Gaussian noise (AWGN) with zero mean and variance σ^{2} . Thus, the received signal can be rewritten as,

$$y = \sqrt{\alpha} \sum_{n=1}^{NM} e^{j(\psi_n^{s} + \psi_n^{r} + \phi_n)} x + w.$$
 (8)

The transmitted signal has a central frequency $f_c = c/\lambda$, where c is the speed of light. The phase shifts $\psi_n^{\rm s}$ and $\psi_n^{\rm r}$ capture the Doppler effect due to the motion of the receiver, where they are expressed as,

$$\psi_n^{\rm s} = -2\pi f_{\rm c} \tau_n^{\rm s}$$
 and (9)

$$\psi_n^{\mathbf{r}} = -2\pi (f_{\mathbf{c}} - f_n) \tau_n^{\mathbf{r}},\tag{10}$$

where $\tau_n^{\rm s}$ denotes the delay of the path between the Tx and the element U_n of the surface, and $\tau_n^{\rm r}$ denotes the delay of the path between U_n and the Rx. If $d_n^{\rm s}$ and $d_n^{\rm r}$ are the distances between the Tx and the element U_n and between U_n and Rx, respectively, then $\tau_n^{\rm s} = d_n^{\rm s}/c$ and $\tau_n^{\rm r} = d_n^{\rm r}/c$. The Doppler frequency experienced by the signal propagating between U_n and the Rx is expressed as,

$$f_n = f_c \frac{v}{c} \frac{\langle \mathbf{d}_n^{\mathbf{r}}, \mathbf{v}_p \rangle}{d_n^{\mathbf{r}} v}, \tag{11}$$

where $\langle .,. \rangle$ represents the inner product operator, \mathbf{v}_p is the pod speed vector, and \mathbf{d}_n^r is the distance vector between the element U_n and the Rx. According to the adopted system configuration, the communication fading channel is dominated by deterministic path loss coefficients, which can be estimated with prior knowledge of the pod's speed and trajectory.

We consider the Cartesian coordinate system as (x,y,z) with origin O as depicted in Fig. 7. For the handover study, we consider two successive cells Cell_1 and Cell_2 intersecting over a distance δ . Let $S_1(0,R,0)$ be the position of the source antenna of Cell_1 and $M_1(R-h,0,0)$ and $M_2(R-h,0,D_s)$ be the positions of the IRSs serving Cell_1 and Cell_2 successively. Also, assume $B(0,0,z_B)$ be the position of the boundary of Cell_1 and $P(0,0,z_P)$ be the position of the pod when it first leaves the overlap area between the two cells. The z-coordinates z_B and z_P can be expressed as,

$$z_{\rm B} = (R - h) \tan \left(\theta + \theta_{\rm t}\right) \tag{12}$$

$$z_{\rm P} = (R - h) \tan \left(\theta + \theta_{\rm t}\right) - \delta. \tag{13}$$

4.3 Achievable Rate Performance

The SNR between the Tx and Rx through the IRS at a location z along the axis of the tube is expressed as,

$$\gamma(z) = \frac{\alpha(z)\beta(z)p_{\rm t}}{\sigma^2},\tag{14}$$

where the factor β incorporates the aggregate effect of the wireless channel phase shifts and is expressed as,

$$\beta(z) = |\sum_{n=1}^{NM} \exp\left(j\left(\phi_n(z) + \psi_n^{\rm s}(z) + \psi_n^{\rm r}(z)\right)\right)|^2.$$
 (15)

Thus, the DL achievable rate can be expressed as [13],

$$R_{\rm D}(z) = \log_2 (1 + \gamma(z)).$$
 (16)

The rate can be further expressed as a function of time t, where t=z/v, equivalently to the expression in (16), as long as the pod is moving. One can deduce that γ depends on $\theta_{\rm t}$ and h, which further motivates tuning them to improve the data link performance of the proposed system.

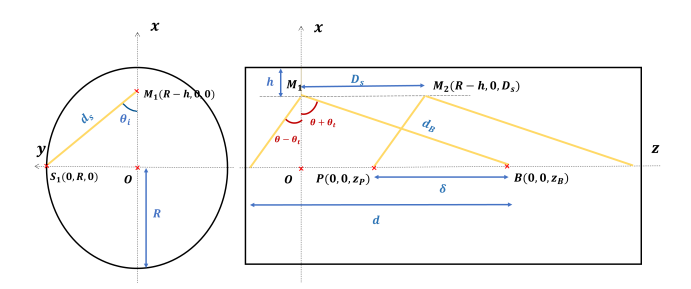


Figure 7: Coordinates of the system components.

5 SINGLE CELL DESIGN

The proposed system configuration relies on a strategic design of the IRS parameters that maximizes the cell range coverage while maintaining a minimum DL rate. The electrical design parameters are $\phi_n(z)$, and the positional-based parameters are h and θ_t . It is worth noting that $\phi_n(z)$ varies with the pod's location, or in other words, with each instant resulting from the pod movement. On the other hand, the IRS positioning parameters are independent of the pod's location. We consider two design phases throughout the design process: phase-shift design and IRS positioning design. In the former, we tune $\phi_n(z)$ to maximize the instantaneous rate, which is necessary to define the IRS operating conditions and increase the DL rate along the cell; hence, the cell coverage can increase. Afterward, the IRS positioning parameters are optimized to maximize the cell coverage considering the tuned $\phi_n(z)$ values. We provide the necessary details of the design problem and optimized solutions in the following subsections.

5.1 Phase-Shift Design

First, we optimize ϕ_n to improve the DL rate. For fixed h and θ_t , the optimization problem is defined as,

$$\max_{\phi_n} \qquad R_{\rm D}\left(\phi_n(z)\right)$$
subject to
$$0 \le \phi_n(z) < 2\pi, n = 1, \dots, NM,$$
(17)

where the constraint defines the $\phi_n(z)$ range in the continuous set $[0, 2\pi]$.

Hence, the optimal $\phi_n(z)$ maximizing $R_{\rm D}\left(\phi_n(z)\right)$, becomes

$$\Phi^*(z) = \arg\max\log_2\left(1 + \frac{\alpha(z)|\mathbf{h}_s^{\mathrm{H}}\mathbf{\Phi}\mathbf{h}_r|^2 p_{\mathrm{t}}}{\sigma^2}\right). \tag{18}$$

Since the summation in (18) is maximum when the exponential terms are equal to 1 for every $n \in \{1, \dots, NM\}$, the

optimal IRS phase shifts when the receiver is at position z along its trajectory are expressed as,

$$\phi_n^*(z) = \phi - (\psi_n^{\rm s}(z) + \psi_n^{\rm r}(z)), \tag{19}$$

where ϕ is an arbitrary value that can be set to 0. Hence, the corresponding optimal rate is expressed as follows,

$$R_{\rm D}^*(z) = \log_2\left(1 + \frac{(NM)^2\alpha(z)p_{\rm t}}{\sigma^2}\right),$$
 (20)

which is in accordance with Snell's Generalized Law. In the following, we derive the necessary conditions for the proposed Hyperloop system to meet the performance constraint.

In order to satisfy the QoS requirements in terms of DL rate, the solution is feasible if it satisfies the following condition:

$$R_{\rm D}\left(\phi_n^*(z)\right) \ge R_{\rm min}.\tag{21}$$

Lemma 1. The optimal design of the IRS-based Hyperloop system (17) exists if and only if the ratio between the IRS area and the corresponding tube cross-sectional serving area, (ρ) , satisfies the following condition,

$$\rho \triangleq \frac{NMab}{\pi (R-h)^2} \ge \sqrt{\frac{16\sigma^2 (2^{R_{\min}} - 1)}{G_t G_r p_t \cos(\theta_i)^4 \cos^2(\theta) \cos(\theta + \theta_t)^2}}.$$
(22)

Proof. The solution in (19) satisfies the rate constraint if and only if,

$$R_{\rm D}^*(z) \ge R_{\rm min}, \ \forall z \in \text{Cell.}$$
 (23)

The DL rate is minimum at the cell edge, i.e., when the receiver is at position B, being the furthest position from the IRS. The signal is subject to a higher pathloss across the cell. Therefore, the condition in (23) is satisfied across the entire cell if and only if

$$R_{\rm D}^*(z_{\rm B}) \ge R_{\rm min}.\tag{24}$$

After defining $d_{\rm s}$ and $d_{\rm B}$ as the distances between the Tx and IRS and between the IRS and the Rx at the cell edge, respectively, then,

$$d_{\rm s} = \frac{R - h}{\cos(\theta_{\rm i})} \tag{25}$$

$$d_{\rm B} = \frac{R - h}{\cos(\theta + \theta_{\rm t})}. (26)$$

Then, we can derive the condition (22) after replacing the distance expressions in the rate expression $R_{\rm D}^*(z_{\rm B})$ and simplifying the rate expression constraint.

One can observe from Lemma 1 that the problem feasibility depends on the IRS choice and serving dimensions. Specifically, one can define the minimum IRS area range, NMab, for a given cross-sectional serving area parameters, i.e., R and h.

5.2 Cell-Coverage Enhancement

To maximize the cell coverage, we optimize the IRS positioning parameters, i.e., θ_t and h. We consider the optimal phase shifts ϕ_n^* derived in the previous section in order to maximize the DL data rate and, thereby, promote wireless coverage expansion. The IRS positioning parameters θ_t and h are fixed and independent of the position of the receiver. Moreover, $R_D(z) \geq R_{\min}, \forall z \in \text{Cell}, \iff R_D(z_B) \geq R_{\min}, \text{ where } R_D(z_B)$ is the minimum value of the rate, reached at the boundary of the cell. Therefore, we should find the parameters θ_t and h at the cell boundary to guarantee meeting the QoS at the entire cell. As such, the problem becomes independent of the receiver's location and can be defined as follows,

$$\max_{h,\theta_{t}} \quad d(h,\theta_{t})$$
subject to
$$C1: R_{D}(h,\theta_{t},z_{B}) \geq R_{\min},$$

$$C2: h_{\min}(\theta_{t}) \leq h \leq h_{\max},$$

$$C3: 0 \leq \theta_{t} < \theta_{t,\max},$$
(27)

where $\theta_{\rm t,max} = \pi/2 - \theta$, $h_{\rm min}(\theta_{\rm t}) = \frac{1}{2}Mb\sin{(\theta_{\rm t})}$ is the minimum allowed distance h to ensure physical (geometric) feasibility of the problem. The maximum value of h is $h_{\rm max} = R - \frac{H_{\rm P}}{2}$, where $H_{\rm P}$ is the height of the pod, assuming that the pod is centrally positioned inside the tube to account for the suspension of the pod. The condition on the tilt angle $\theta_{\rm t} + \theta < \pi/2$ must be satisfied in order to avoid the IRS radiating towards the ceiling of the tube and creating reflections. It is worth mentioning that the constraint (C2) cannot be valid unless $h_{\rm min} \leq h_{\rm max}$ which is equivalent to $\sin{(\theta_{\rm t})} \leq \frac{2R-H_{\rm P}}{Mb}$. Therefore, in order to ensure $h_{\rm min} \leq h_{\rm max}$, the following condition has to be satisfied,

$$Mb \le 2R - H_{\rm P}.\tag{28}$$

First, we need to write the expression of the rate $R_{\rm D}\left(h, \theta_{\rm t}, z_{\rm B}\right)$ as a function of the optimization parameters $\theta_{\rm t}$ and h to study the problem (17) the feasibility. The distance $d_{\rm s}$ between the Tx and IRS satisfies the following equation,

$$d_{\rm s}^2 = (SM)^2 = (R - h)^2 + R^2.$$
 (29)

Considering that $\cos\theta_{\rm i}=\frac{R-h}{d_{\rm s}}$ as can be seen in Fig. 7, we can simplify the rate expression by assembling the system's constants in one constant Ω . The rate is thus re-expressed as,

$$R_{\rm D}(h, \theta_{\rm t}, z_{\rm B}) = \log_2 \left(1 + \Omega \frac{\cos(\theta + \theta_{\rm t})^2}{(R^2 + (R - h)^2)^2} \right),$$
 (30)

where Ω is a constant defined as,

$$\Omega = \frac{G_{\rm t}G_{\rm r}}{(4\pi)^2} (NMab)^2 \cos^2(\theta) \frac{p_{\rm t}}{\sigma^2}.$$
 (31)

Then, by using (30), we can express the rate constraint (C1) in Problem (27) can be transformed in terms of h as follows,

$$h \ge g(\theta_{\rm t}) \triangleq R - \sqrt{\sqrt{\frac{\Omega}{2^{R_{\rm min}} - 1}} \cos(\theta + \theta_{\rm t}) - R^2}.$$
 (32)

The inequality (32) is valid and does not contradict the system feasibility since $g(\theta_t)$ is always less than the tube

radius R. In the following, we define the rate feasibility problem in terms of conditions on the design parameters.

Lemma 2. The rate constraint $R_D(h, \theta_t, z_B) \ge R_{\min}$ is valid if and only if $\theta_t \le \theta_{th}$, where,

$$\theta_{\rm th} = \arccos\left(R^2\sqrt{\frac{2^{R_{\rm min}} - 1}{\Omega}}\right) - \theta.$$
 (33)

Proof. The expression under the square root in (32) must be positive. Therefore,

$$\sqrt{\frac{\Omega}{2^{R_{\min}} - 1}} \cos(\theta + \theta_{t}) - R^{2} \ge 0$$

$$\iff \cos(\theta + \theta_{t}) \ge R^{2} \sqrt{\frac{2^{R_{\min}} - 1}{\Omega}}$$

$$\iff \theta_{t} \le \arccos\left(R^{2} \sqrt{\frac{2^{R_{\min}} - 1}{\Omega}}\right) - \theta. \tag{34}$$

The condition derived at Lemma (2) implies that rotating the IRS more than the threshold $\theta_{\rm th}$ results in long transmission distances and thus low SNR, which can not fulfill the required data rate. Therefore, the system is incapable of keeping the minimum required QoS under the given conditions in terms of transmit power, antenna gains, and IRS parameters.

Lemma 3. The maximum rate that can be supported at the cell boundary is expressed as,

$$R_{\text{maxB}} = \log_2\left(1 + \frac{\Omega}{R^4}\right). \tag{35}$$

Proof. The argument of the function arccos in (33) is conditioned as follows,

$$R^2 \sqrt{\frac{2^{R_{\min}} - 1}{\Omega}} < 1 \iff R_{\min} < \log_2 \left(1 + \frac{\Omega}{R^4}\right).$$
 (36)

As a result, from the inequality $R_{\min} \leq R_{\max B}$, we can deduce that there is a tradeoff between the cell range and minimum rate regarding the radius dimension of the tube. Increasing the radius of the tube R increases the cell range linearly, as can be seen in (1). However, the maximum possible rate $R_{\max B}$ decreases, leading to a reduced feasible space.

Therefore, after the reformulation of the constraint in (32), problem (27) can be rewritten as,

$$\max_{h,\theta_{t}} d$$
subject to
$$f(\theta_{t}) \leq h \leq h_{\max}$$

$$0 \leq \theta_{t} < \min(\theta_{t,\max}, \theta_{th}) \triangleq \theta_{F},$$
(37)

where the function f is defined as,

$$f(\theta_{t}) = \max(h_{\min}(\theta_{t}), g(\theta_{t})). \tag{38}$$

The distance d is increasing in θ_t and decreasing in h. According to the last problem formulation, the choice of h does not affect the parameter θ_t . Therefore, the optimal

choice for h is $h^* = f(\theta_t)$. In this case, the problem (37) can be rewritten as,

$$\max_{\theta_{t}} \quad d(f(\theta_{t}), \theta_{t})
\text{subject to} \quad 0 \leq \theta_{t} < \theta_{F}.$$
(39)

The problem (27) is reduced to a one-dimensional optimization problem (39) easier and faster to solve. The function $d\left(f(\theta_{\rm t}),\theta_{\rm t}\right)$ is a non-smooth function with possibly multiple maxima. First, one can prove the increasing characteristics of both functions $h_{\min}(\theta_{\rm t})$ and $g(\theta_{\rm t})$ by studying their behavior in the $\theta_{\rm t}$ interval, i.e., since $\theta_{\rm t} \in [0,\pi/2[$. Then, the problem can be solved over different intervals according to the relative positions of h_{\min} and g. To this end, there are three possible scenarios defined as follows:

- Case 1: $g(\theta_{\rm t}) \geq h_{\min}(\theta_{\rm t}), \forall \ 0 \leq \theta_{\rm t} < \theta_{\rm F} \ \text{if} \ g(0) \geq h_{\min}(0) \ \text{and} \ g\left(\theta_{\rm F}\right) \geq h_{\min}\left(\theta_{\rm F}\right)$
- Case 2: $g(\theta_{\rm t}) \leq h_{\min}(\theta_{\rm t}), \forall \ 0 \leq \theta_{\rm t} < \theta_{\rm F} \ {\rm if} \ g(0) \leq h_{\min}(0) \ {\rm and} \ g\left(\theta_{\rm F}\right) \leq h_{\min}\left(\theta_{\rm F}\right)$
- Case 3: The functions g and h_{\min} intersect at a point $\theta_0 \in [0, \theta_{\mathrm{F}}]$ if $\{g(0) \geq h_{\min}(0) \text{ and } g(\theta_{\mathrm{F}}) \leq h_{\min}(\theta_{\mathrm{F}})\}$ or $\{g(0) \leq h_{\min}(0) \text{ and } g(\theta_{\mathrm{F}}) \geq h_{\min}(\theta_{\mathrm{F}})\}$

When the problem is identified under Case 1 or Case 2, the problem is solved over the interval $[0, \theta_{\rm F}]$. On the other hand, if the problem is identified under Case 3, the problem is solved over $[0, \theta_0]$ and $[\theta_0, \theta_F]$. Therefore, over each interval, Problem (39) is a single variable minimization problem with a differentiable objective function and boundary constraints. If the system setup falls under Case 1 or Case 2, the stationary points of the objective function $d(f(\theta_t), \theta_t)$ are determined (if existent). The objective function is then evaluated at these stationary points and at the boundary of the interval $[0, \theta_F]$. Otherwise, if the system setup falls under Case 3, the objective function is further evaluated at the intersection point θ_0 . The stationary points are determined over both intervals $[0, \theta_0]$ and $[\theta_0, \theta_F]$. The optimal tilting angle is the angle θ_t that maximizes the objective function. This part is summarized in Algorithm

Algorithm 1 Solution of Problem (39)

$$\begin{split} & \textbf{Require: } \theta_{\mathrm{F}}, g, h_{\mathrm{min}} \\ & \textbf{if Case 1 or Case 2 then} \\ & f = \max\left(g, h_{\mathrm{min}}\right) \\ & \theta_{\mathrm{s}} = \left\{\theta_{\mathrm{t}} \in (0, \theta_{\mathrm{F}}), d'\left(f(\theta_{\mathrm{t}}), \theta_{\mathrm{t}}\right) = 0\right\} \\ & \textbf{else if Case 3 then} \\ & \theta_{0} = \left\{\theta_{\mathrm{t}} \in (0, \theta_{\mathrm{F}}), h_{\mathrm{min}}(\theta_{\mathrm{t}}) = g(\theta_{\mathrm{t}})\right\} \\ & f = \max\left(g, h_{\mathrm{min}}\right) \\ & \theta_{\mathrm{s}} = \left\{\theta_{\mathrm{t}} \in (0, \theta_{0}), d'\left(f(\theta_{\mathrm{t}}), \theta_{\mathrm{t}}\right) = 0\right\} \cup \left\{\theta_{\mathrm{t}} \in (\theta_{0}, \theta_{\mathrm{F}}), d'\left(f(\theta_{\mathrm{t}}), \theta_{\mathrm{t}}\right) = 0\right\} \\ & \textbf{end if} \\ & \theta_{\mathrm{t}}^{*} = \arg\max_{\theta_{\mathrm{t}}} d\left(f(\theta_{\mathrm{t}}), \theta_{\mathrm{t}}\right), \theta_{\mathrm{t}} \in \left\{0, \theta_{0}, \theta_{\mathrm{s}}, \theta_{\mathrm{F}}\right\} \end{split}$$

6 MULTI-CELL SYSTEM

After providing a design framework for a single cell, we now focus on the multi-cell configuration, which considers the overlap between successive cells and its effect on the

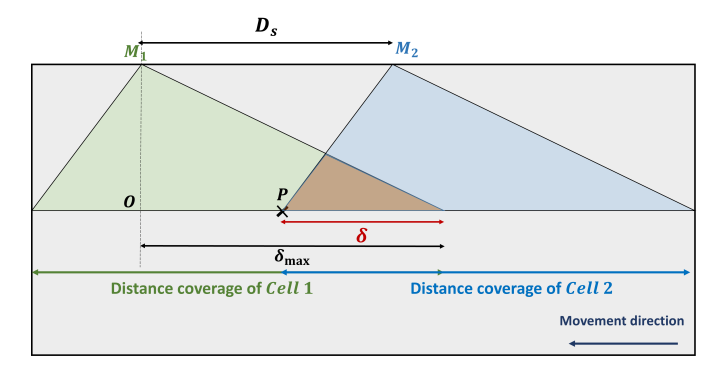


Figure 8: Successive cells intersection.

handover process. The objective of the handover process is to achieve continuous service delivery to the moving pod during cell-crossing with sufficient QoS. Although handover decision criteria such as the appropriate target cell or moment of connection are determined beforehand at the CS, we focus on addressing the high number of handovers during travel as one of the particular limitations of Hyperloop communication system. Since handover performance is one of the main challenges in high mobility scenarios, the system should limit the handover rate to minimize communication errors. Although the handover process in Hyperloop is deterministic, it is important to provide an optimized network planning.

In order to avoid confusion of terms during the design approach, a cell corresponding to an AP is defined by the area that this AP can cover based on the single-cell design, even if there is no signal broadcasting. In Fig. 8, two successive cells are depicted, Cell_1 and Cell_2 and their corresponding IRSs, M_1 and M_2 . The overlap distance δ is the design parameter representing the boundary of the handover phase.

6.1 Problem Formulation

In this section, we tune the range of the overlap area δ in order to minimize the handover rate while keeping the rate at position P greater than a threshold, where P corresponds to the position of the pod when it first leaves the overlap area. The corresponding optimization problem can be written as,

$$\begin{array}{ll} \min\limits_{\delta} & H_{\rm r}(\delta) \\ {\rm subject\ to} & R_{\rm D}(\delta,z_{\rm P}) \geq R_{\rm min} \\ & \delta_{\rm min} \leq \delta \leq \delta_{\rm max}. \end{array} \tag{40}$$

The first constraint of Problem (40) is used to maintain the rate $R_{\rm D}(\delta,z_{\rm P})$ at position P greater than a minimum value $R_{\rm min}$, where $R_{\rm D}(\delta,z_{\rm P})=\log_2\left(1+\gamma_{\rm P}\right)$ and $\gamma_{\rm P}$ is the SNR. The second constraint ensures that the distance dedicated for handover δ is restricted by two limits $\delta_{\rm min}$ and $\delta_{\rm max}$. The lower bound $\delta_{\rm min}=vt_{\rm O}$ ensures a minimum overlap between successive cells to guarantee a minimum time interval $t_{\rm O}$ for handover execution. The value of $\delta_{\rm min}$ depends on the handover algorithm adopted by the CS and can be set accordingly. The upper bound is $\delta_{\rm max}=(R-h)\tan\left(\theta+\theta_{\rm t}\right)$. The upper bound of the overlap distance is here set to $\delta_{\rm max}$, where P would be superimposed with position O of

Fig. 8. At this position, the signal coming from $Cell_1$ has the maximum SNR across the cell coverage area. Therefore, increasing δ beyond δ_{\max} would increase the handover rate with lower signal quality.

The choice of position P is mainly based on the fact that no communication interruption or signal deterioration should occur between successive cells. During handover, the receiver is served simultaneously by the APs of Cell_1 and Cell_2 and connects to the signal with maximum SNR. In order to ensure a sufficient QoS when the pod leaves the overlap area and can no longer acquire a link from Cell_2 , the receiver will only be served by Cell_1 . Since the handover phase is complete at this point, the receiver cannot rely on signal diversity to keep an acceptable QoS. For this reason, it is necessary to keep the rate at the transition point P greater than a threshold R_{\min} .

6.2 Multi-Cell Design

In order to solve problem (40), we investigate the behavior of the objective function and constraints as a function of the optimization parameter δ . The handover rate as expressed in (5) is increasing in δ . Thus, minimizing the handover rate is equivalent to minimizing the overlap distance δ . Consequently, the pod stops receiving signals from the serving cell when the handover phase is complete. The DL signal is coming from the source of the target cell, Cell₁ of Fig. 8. Therefore, the SNR of the signal at position P is expressed as $\gamma_P = \gamma_1$, where γ_1 is the SNR of the signal coming from Cell₁. Let $d_{\rm s1}$ be the distance of the direct paths between S_1 and M_1 , and d_P the distance of the reflected paths between M_1 and P, as depicted in Fig. 7. These distances can be expressed as follows,

$$d_{\rm s1}^2 = (R - h)^2 + R^2 \tag{41}$$

$$d_{\rm P}^2 = (R - h)^2 + z_{\rm P}^2. \tag{42}$$

Using the SNR expression in (14) and the expression of the coordinate $z_{\rm P}$ found in (13), the SNR γ_1 can be expressed as function of δ as,

$$\gamma_1(\delta) = \frac{\Omega_{\mathcal{A}}}{(R-h)^2 + ((R-h)\tan(\theta + \theta_{\mathsf{t}}) - \delta)^2} \tag{43}$$

and Ω_A is a constant expressed as,

$$\Omega_{\mathcal{A}} = \Omega \left(\frac{R - h}{R^2 + (R - h)^2} \right)^2. \tag{44}$$

Hence, the achievable rate at location P is expressed in terms of δ as,

$$R_{\rm D}(\delta, z_{\rm P}) = \log_2 \left(\frac{\Omega_{\rm A}}{(R-h)\tan(\theta + \theta_{\rm t}) - \delta} \right).$$
 (45)

As a result of the rate expression in (45), the rate constraint in (40) can be transformed to a constraint on the distance δ as follows,

$$\delta \ge \delta_{\rm th},$$
 (46)

where $\delta_{\rm th}$ is the limit distance defined as,

$$\delta_{\rm th} = (R - h) \tan (\theta + \theta_{\rm t}) - \sqrt{\frac{\Omega_{\rm A}}{2^{R_{\rm min}} - 1} - (R - h)^2}.$$
 (47)

Lemma 4. The rate constraint in (40) is valid if and only if $R_{\min} \leq R_{\max}$ that is defined as follow,

$$R_{\text{maxB}} = \log_2 \left(1 + \frac{\Omega_{\text{A}}}{(R-h)^2} \right). \tag{48}$$

Proof. The threshold $\delta_{\rm th}$ on the distance δ exists if and only if the expression under the square root is positive, i.e.,

$$\frac{\Omega_{\rm A}}{2^{R_{\rm min}} - 1} - (R - h)^2 \ge 0. \tag{49}$$

The minimum rate requirement $R_{\rm min}$ is constrained by a maximum value that cannot exceed $R_{\rm maxB}$ for the considered system parameters. Similarly to the conclusion drawn in the previous section, when the radius decreases, the limit $R_{\rm maxB}$ increases, leading to an expansion of the feasibility space of (40). However, according to (1), the cell coverage decreases, leading to more frequent handovers. As a result of the constraint re-evaluation in (46), (40) can be reformulated as,

$$\min_{\delta} \quad \delta
\text{subject to} \quad \max(\delta_{\min}, \delta_{\text{th}}) \le \delta \le \delta_{\max}.$$
(50)

Therefore, the optimal solution is,

$$\delta^* = \max\left(\delta_{\rm th}, \delta_{\rm min}\right). \tag{51}$$

7 SIMULATION RESULTS

In this section, we evaluate the benefits of implementing the proposed system configuration through different simulation examples. The objective is to study the impact of the optimized system parameters and the IRS specifications on both the cell coverage and the handover rate. The simulation parameters² are summarized in Table. 1.

| Parameter | Value | Parameter | Value |
|------------|-------------|-------------------|-----------------------------|
| R | 2 m | p_t | 1 W |
| $H_{ m P}$ | 1.10 m | σ^2 | -80 dBm |
| a,b | $\lambda/3$ | G_t | 35 dB |
| N | 50 | G_r | 15 dB |
| M | 34 | $\theta_{ m max}$ | $\pi/2 - \theta - \epsilon$ |
| f_c | 60 GHz | ϵ | 1^o |

Table 1: Simulation parameters

7.1 Single-Cell Design

We start by studying the single-cell coverage performance, the impact of system parameters on its performance, and the design benefits. Specifically, we study the variation of optimized parameters $\theta_{\rm t}$, h and d versus the QoS constraint $R_{\rm min}$ for different possible ranges of IRS scanning abilities as shown in Fig. 9, Fig. 10 and Fig. 11, respectively. Firstly, we observe a constant maximum coverage between 109 m and 114 m that can be obtained for $R_{\rm min}$ is less than a certain threshold. This threshold depends on the angle θ . This maximum distance is achieved when $\theta_{\rm t}=\theta_{\rm t,max}$ and h is at its minimum values, as shown in Fig. 9. At low $R_{\rm min}$ range, $\theta_{\rm t}$ and h are tuned to maximize the distance

2. The parameters of the metasurface are acquired from [35] and the tube dimension is the same as HyperloopTT technology prototype [17].

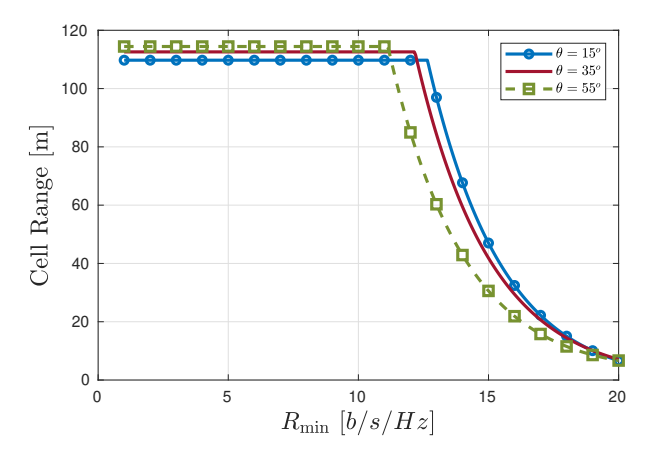


Figure 9: Cell range versus R_{\min} .

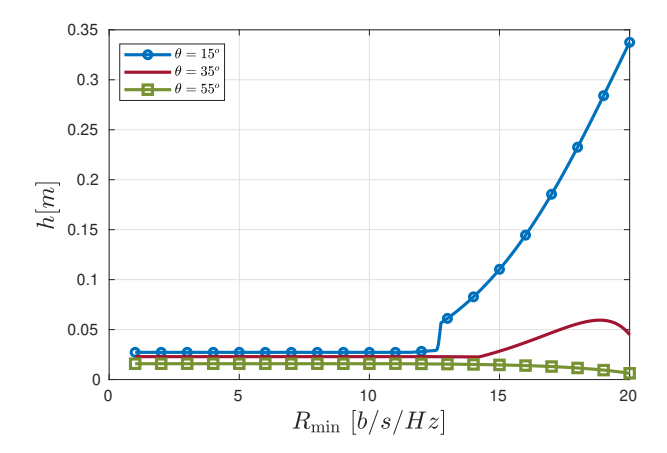


Figure 10: Distance h versus R_{\min} .

without violating this rate constraint given a minimum hand a maximum θ_t . As R_{\min} increases, the system tunes the parameters to satisfy the increasing required rate at the expense of decreased cell coverage, considering the increasing behavior of $R_{\rm D}(z_{\rm B})$ with h and decreasing behavior with $\theta_{\rm t}$. Hence, $\theta_{\rm t}$ keeps decreasing, and h keeps increasing to maintain R_{\min} as can be depicted in Fig. 10 and Fig. 11. For instance in Fig. 10, for $\theta = 15^{\circ}$, h increases to maintain $R_{\rm min}$, when $R_{\rm min} \geq 13\,{\rm b/s/Hz}$. The behavior of the optimal elevation distance h changes after a certain minimum rate is required. When $R_{\rm min} < 13\,{\rm b/Hz/s}$, the optimal distance is $h_{\min}(\theta_t)$ and is constant for all R_{\min} . Then, when the minimum rate exceeds $13 \,\mathrm{b/Hz/s}$, $h_{\min}(\theta_{\mathrm{t}})$ is incapable of meeting these higher requirements, the distance h starts increasing to reduce the transmission distance and therefore increase the rate. For $\theta=35^{\circ}$, the distance h increases to maintain R_{\min} then starts decreasing to increase the cell coverage since the decreasing behavior of θ_t is capable of maintaining R_{\min} . The difference in the behavior between IRSs with different scanning angles is explained by the fact that a higher θ requires a smaller tilting angle θ_t and, therefore, a shorter distance h since it is increasing in θ_t .

Second, Fig. 9 shows that the angular scanning range of the IRS θ does not significantly impact the system's performance in terms of cellular coverage. In fact, the coverage distance d increases with the scanning angle θ , with a

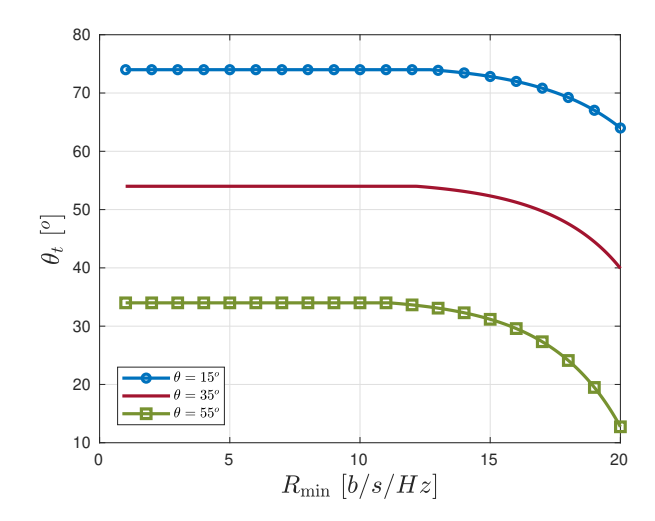


Figure 11: Tilting angle versus R_{\min} .

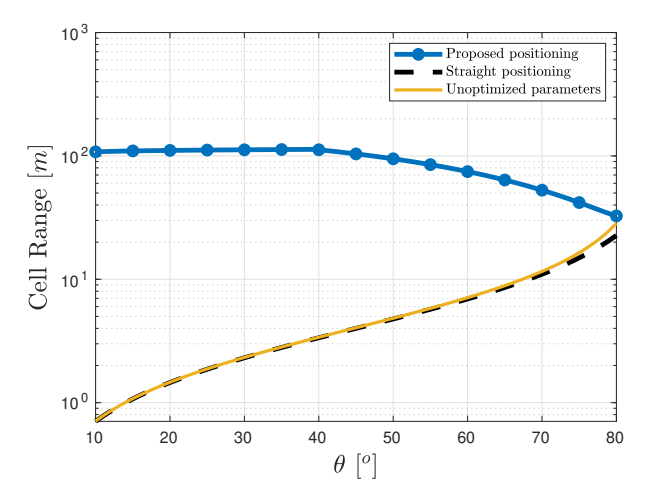


Figure 12: Benchmark comparison between the proposed design, the straight positioning and the unoptimized positioning.

maximum gain of 5 m when $\theta = 55^{\circ}$ compared to $\theta = 15^{\circ}$, corresponding to a 4 % increase in distance, for small values of R_{\min} . On the other hand, when R_{\min} is higher, the performance gain achieved for smaller scanning angles θ is slightly more significant than for lower R_{\min} . This can be explained by the increased channel gain proportional to $\cos(\theta)^2$; with smaller θ , the system can better satisfy the rate requirements. Therefore, an IRS with lower scanning capabilities is preferred. Smaller θ increases the channel gain, while the tilting position is capable of compensating for the coverage loss. We can deduce that the proposed system architecture and the corresponding design do not rely on the high specifications of the IRS since different θ values can achieve the same performance in terms of cell coverage. Low IRS angular scanning ranges can achieve significantly large cell coverage distances. The design of the proposed architecture relying on IRS tilting does not need unrealistic metasurface parameters and does not impose heavy constraints on the IRS to maintain a proper operation. The system can be designed to achieve the required performance while keeping certain flexibility on the metasurface.

To better evaluate the benefit of the system choice, we provide in Fig. 12, a comparison between the proposed positioning, the straight positioning, i.e. $\theta_{\rm t,st}=0, h_{\rm st}=0$ (horizontal IRS) and an unoptimized setup using $\theta_{t,unop}$ = $\theta_{\rm t,max}/2$ and $h_{\rm unop}=h_{\rm min}\,(\theta_{\rm t,unop}).$ In fact, the straight positioning of the IRS also represents the typical setup of APs assisted with beam-steering capabilities to avoid multipath and signal reflections. The minimum rate is set to 10 b/s/Hz. Firstly, as previously observed, the variations of the proposed positioning design are not significant because the effect of the IRS scanning angle has a negligible effect on the cell range for $\theta < 60^{\circ}$. Specifically, we observe that the variation in d does not exceed 10 m across the range of θ , $[10^{\circ}, 50^{\circ}]$. Higher values of θ lead to a significant decrease in the channel gain that can be compensated by a decrease in the transmission distance. Secondly, the cell coverage ranges achieved by the proposed IRS positioning are significantly higher than the straight positioning and the unoptimized positioning, with a difference that can reach 100 m. The regular positioning reaches 20 m cell range at most with very wide scanning angles that cannot be achieved in practical scenarios. Since the objective of this work is coverage maximization rather than rate improvement, the lower spectral efficiency achieved with the proposed setup is not considered a limitation as long as the minimum required QoS is guaranteed. Moreover, the straight and the unoptimized setups reach comparable performances implying that without an appropriate design of the IRS parameters h and θ_t , the system cannot achieve cell coverage performance.

In this simulation example, we compare our proposed setup to using only the AP for communication, as shown in Fig. 13. To provide a fair comparison, we assume a wider transmitted signal beam for the benchmark to cover the same cell coverage as our system. However, the benchmark setup is susceptible to signal degradation from multipath interference caused by signal bounces on the tube wall. To further emphasize the value of our proposed architecture, we assume that the benchmark is able to perform ideal interference cancellation. Fig. 13 shows the superiority of our proposed setup, which is due to the signal degradation resulting from widening the beam to maintain the same cell coverage. Therefore, our proposed AP-IRS setup can provide relatively wide coverage by steering a narrow signal beam to track the moving pod, while maintaining high signal quality and avoiding multipath interference.

7.2 Multi-Cell Design

In this section, we study the Hyperloop multi-cell performance and design while considering the same simulation parameters of the previous section and $\theta_{\rm t}=55^{\circ}$.

In the first simulation example, we investigate the rate at position P and the handover rate versus the optimal overlap distance, as shown in Fig. 14. We assume two different cell configurations; first, when the cell range is $d=94\,\mathrm{m}$ with a minimum rate $R_{\min}=12\,\mathrm{b/s/Hz}$ and second, when $d=45\,\mathrm{m}$ with a minimum rate $R_{\min}=14\,\mathrm{b/s/Hz}$. The results show that lower rates are achieved at position P for the same overlap distance when the cell range increases,

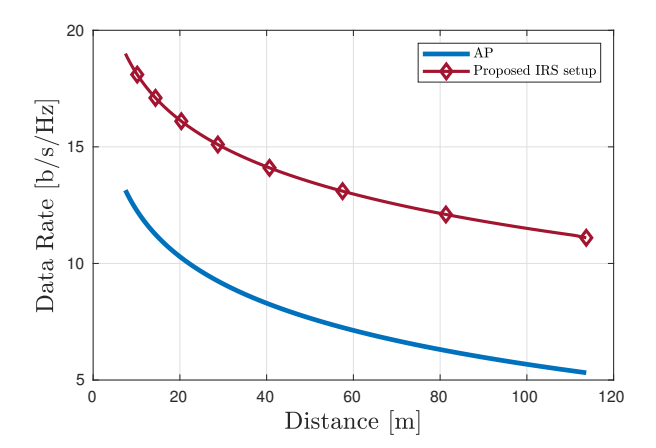


Figure 13: Benchmark comparison.

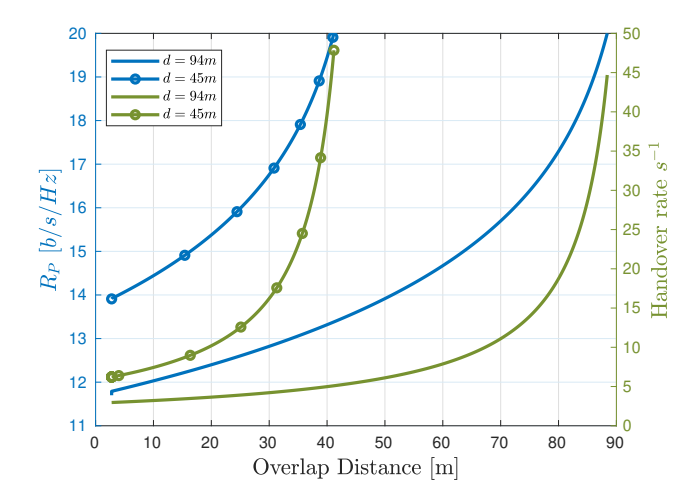


Figure 14: Rate at position P and handover rate versus δ .

causing the rate deterioration. Although the rate $R_{\rm P}$ increases with δ , this profit is achieved at the expense of more frequent handovers. Therefore, there is a tradeoff between the minimum required rate and the number of handovers executed along the traveled path.

In the second simulation example, we study the number of wireless cells versus the total path distance traveled by the pod for two different overlap distances $\delta = 7 m$ and $\delta = 30 \, m$ assuming $d = 94 \, \text{m}$, as shown in Fig. 15. The increasing behavior of the curve is expected because covering longer distances requires deploying more wireless cells to ensure uninterrupted communication between the Tx and Rx. Additionally, the number of cells is less when $\delta = 7 m$ and the distance gap between the two cases becomes more significant when the total distance $D_{\rm T}$ increases. For instance, when $D_{\rm T}=9\,{\rm km}$, the total path requires 40 additional cells when $\delta = 30\,\mathrm{m}$ compared to the case $\delta = 7 \,\mathrm{m}$. However, this deployment cost is compensated by increased spectral efficiency. In fact, when $\delta = 7 \,\mathrm{m}$, the rate at position P is $R_{\rm P} = 11.9 \,\mathrm{b/s/Hz}$ while $R_{\rm P} = 12.9 \, {\rm b/s/Hz}$ when $\delta = 30 \, {\rm m}$.

The previous simulation results indicate that increasing the overlap distance increases the cost of the system due to the higher number of APs required to ensure full network coverage. However, at the same time, expanding the overlap distance helps reduce the complexity of the handover process at the CS because the system can tolerate longer handover delays. Therefore, if the system can ensure a fast handover execution technique at the CS, we can tolerate deploying fewer APs along the tube length. To sum up, depending on the design and available resources, higher complexity and/or cost are either imposed on the network inside the tube or the network outside the tube.

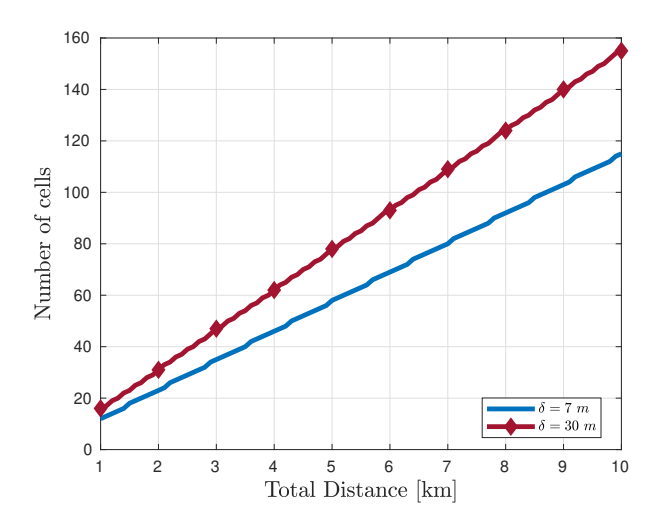


Figure 15: Number of deployed cells versus the travel distance.

Considering that data transmission between the Tx and Rx is interrupted during the switching of the IRS phase shifters, we evaluate the effect of the IRS switching time on the system performance. If the size of the antenna is $w=13.8\,mm$ as in [27], the visibility time is $t_{\rm Data}=\frac{w}{v}=50\,\mu{\rm s}$. Fast switching is possible for IRSs operating in the millimeter band [36]. Therefore, if the silence time is $\tau_{\rm switch}=40\,{\rm ns}$, the percentage of time when data downloading is occurring is $\eta=\frac{50}{50+40.10^{-3}}=99.92\%$. Thus, data transmission between the core network and the train happens 99.92 % of the time. It is worth mentioning that using electric field stimuli, shorter switching intervals can be achieved [37] such as 2 ns as in [38] and 4.5 ns as in [39]. In this case, quasi-real transmission can be carried out.

8 Conclusion

In this paper, we proposed a novel wireless network architecture and design for the inner tube communication system of Hyperloop, where IRS-beam steering is adopted to track the moving pod and avoid signal reflections inside the steel-made tube. Moreover, the successive IRSs are arranged in a tilting position in order to maximize the wireless cell coverage. Adopting this architecture ensures significant flexibility over IRS choice since IRSs with different scanning angles achieve similar performance. In terms of cell coverage, it outperforms the regular architecture with the straight positioning of the IRS on the tube wall. Moreover, the optimized design of the overlap distance dedicated to the handover process between successive APs contributes to reducing the deployment cost in terms of the number of APs, without violating QoS constraints. On the other hand,

the switching time of the IRS is an important factor that affects the system's performance, especially in the case of Hyperloop, which moves at very high speeds. As future work, channel estimation techniques could be explored to adapt the IRS system to uncertainties and discrepancies. The overall system design helps reduce the deployment cost and the complexity of its components. The optical backhauling, centralized operation and appropriate APs installation inside the tube are key steps towards minimizing the handover delay and coping with other challenges arising from the extremely high speed of the pod and the unique tube environment.

REFERENCES

- [1] E. Musk, "Hyperloop alpha," SpaceX: Hawthorne, CA, USA, 2013.
- [2] N. A. Alexander and M. M. Kashani, "Exploring bridge dynamics for ultra-high-speed, Hyperloop, trains," in *Structures*, vol. 14. Elsevier, 2018, pp. 69–74.
- [3] W. Hedhly, O. Amin, B. Shihada, and M.-S. Alouini, "Hyperloop Communications: Challenges, Advances, and Approaches," *IEEE Open. J. Commun. Soc.*, 2021.
- [4] Q. Wu and R. Zhang, "Towards smart and reconfigurable environment: Intelligent reflecting surface aided wireless network," *IEEE Commun. Mag.*, vol. 58, no. 1, pp. 106–112, 2019.
- [5] H.-H. Hsiao, C. H. Chu, and D. P. Tsai, "Fundamentals and applications of metasurfaces," Small. Met., vol. 1, no. 4, p. 1600064, 2017.
- [6] W. Pan, C. Huang, P. Chen, M. Pu, X. Ma, and X. Luo, "A beam steering horn antenna using active frequency selective surface," *IEEE Trans. Ant. Propag.*, vol. 61, no. 12, pp. 6218–6223, 2013.
- [7] T. Jiang, Z. Wang, D. Li, J. Pan, B. Zhang, J. Huangfu, Y. Salamin, C. Li, and L. Ran, "Low-DC voltage-controlled steering-antenna radome utilizing tunable active metamaterial," *IEEE Trans. Microw. Theo. Techn.*, vol. 60, no. 1, pp. 170–178, 2011.
- Theo. Techn., vol. 60, no. 1, pp. 170–178, 2011.
 [8] H. Li, D. Ye, F. Shen, B. Zhang, Y. Sun, W. Zhu, C. Li, and L. Ran, "Reconfigurable diffractive antenna based on switchable electrically induced transparency," *IEEE Trans. Microw. Theo. Tech.*, vol. 63, no. 3, pp. 925–936, 2015.
- [9] X. Wan, M. Q. Qi, T. Y. Chen, and T. J. Cui, "Field-programmable beam reconfiguring based on digitally-controlled coding metasurface," Sci. Rep., vol. 6, no. 1, pp. 1–8, 2016.
- [10] A. Roze, M. Hélard, M. Crussière, and C. Langlais, "Millimeterwave digital beamsteering in highly line-of-sight environments for massive mimo systems," in Wirel. World. Res. Forum. Meet., vol. 35, 2015.
- [11] F. Sohrabi and W. Yu, "Hybrid digital and analog beamforming design for large-scale antenna arrays," *IEEE J. Sel. Top. Sig. Proc.*, vol. 10, no. 3, pp. 501–513, 2016.
- [12] Q. Wu and R. Zhang, "Beamforming optimization for intelligent reflecting surface with discrete phase shifts," in *IEEE Int. Conf. Acoust., Speech. Sig. Process.*, 2019, pp. 7830–7833.
- [13] H. Guo, Y.-C. Liang, J. Chen, and E. G. Larsson, "Weighted sum-rate maximization for reconfigurable intelligent surface aided wireless networks," *IEEE Trans. Wirel. Commun.*, vol. 19, no. 5, pp. 3064–3076, 2020.
- [14] Q. Wu and R. Zhang, "Intelligent reflecting surface enhanced wireless network via joint active and passive beamforming," *IEEE Trans. Wirel. Commun.*, vol. 18, no. 11, pp. 5394–5409, 2019.
- [15] C. Huang, A. Zappone, G. C. Alexandropoulos, M. Debbah, and C. Yuen, "Reconfigurable intelligent surfaces for energy efficiency in wireless communication," *IEEE Trans. Wirel. Commun.*, vol. 18, no. 8, pp. 4157–4170, 2019.
- [16] V. Jamali, G. C. Alexandropoulos, R. Schober, and H. V. Poor, "Low-to-zero-overhead IRS reconfiguration: Decoupling illumination and channel estimation," *IEEE Commun. Let.*, vol. 26, no. 4, pp. 932–936, 2022.
- pp. 932–936, 2022. [17] "Hyperloop TT Technology," https://www.hyperlooptt.com/technology/.
- [18] J. Zhang, L. Liu, Z. Li, T. Zhou, C. Qiu, B. Han, D. Wang, and Z. Piao, "Two novel structures of broadband wireless communication for high-speed flying train in vacuum tube," in 28th Wirel. opt. Commun. Conf. IEEE, 2019, pp. 1–5.

- [19] B. Wei, Z. Li, L. Liu, and J. Wang, "Field distribution characteristics of leaky-wave system in the vacuum tube for high-speed rail," in IEEE 12th Int. Symp. Ant. Propag. EM. Theor. (ISAPE), Hangzhou, China, Dec. 2018, pp. 1–3.
- [20] C. Qiu, L. Liu, Y. Liu, Z. Li, J. Zhang, and T. Zhou, "Key technologies of broadband wireless communication for vacuum tube high-speed flying train," in 89th Veh. Technol. Conf. IEEE, 2019, pp. 1–5.
- [21] B. Han, J. Zhang, L. Liu, and C. Tao, "Position-based wireless channel characterization for the high-speed vactrains in vacuum tube scenarios using propagation graph modeling theory," *Radio Sci.*, vol. 55, no. 4, p. e2020RS007067, 2020.
- [22] J. Zhang, L. Liu, K. Wang, B. Han, Z. Piao, and D. Wang, "Analysis of the effective scatters for hyperloop wireless communications using the geometry-based model," in *Int. Conf. Mach. Learn. Cyber. Sec.* Springer, 2020, pp. 87–97.
- [23] L. Han, H. Wu, and X. Chen, "Wireless network architecture for evacuated tube transportation system," China. Commun., vol. 17, no. 10, pp. 206–217, 2020.
- [24] C. Qiu, L. Liu, B. Han, J. Zhang, Z. Li, and T. Zhou, "Broadband wireless communication systems for vacuum tube high-speed flying train," App. Sci., vol. 10, no. 4, p. 1379, 2020.
- [25] X. Huang, F. Yang, J. Song, and Z. Han, "An optical communication approach for ultra-high-speed train running in evacuated tube: Potentials and challenges," *IEEE Wirel. Commun.*, 2021.
- [26] Y. Hwang and J. Shin, "Group handover management for v2x in moving cell based lte-advanced system," in *IEEE Int. Conf. Inf. Commun. Tech. Converg. (ICTC)*, 2015, pp. 1054–1057.
- [27] M. Ohira, A. Miura, and M. Ueba, "60-ghz wideband substrate-integrated-waveguide slot array using closely spaced elements for planar multisector antenna," *IEEE Trans. Ant. Propag.*, vol. 58, no. 3, pp. 993–998, 2009.
- [28] X. Lin, R. K. Ganti, P. J. Fleming, and J. G. Andrews, "Towards understanding the fundamentals of mobility in cellular networks," *IEEE Trans. Wirel. Commun.*, vol. 12, no. 4, pp. 1686–1698, 2013.
- [29] R. Arshad, H. ElSawy, S. Sorour, T. Y. Al-Naffouri, and M.-S. Alouini, "Handover management in 5G and beyond: A topology aware skipping approach," *IEEE Access.*, vol. 4, pp. 9073–9081, 2016.
- [30] W. Tang, M. Z. Chen, J. Y. Dai, Y. Zeng, X. Zhao, S. Jin, Q. Cheng, and T. J. Cui, "Wireless communications with programmable metasurface: New paradigms, opportunities, and challenges on transceiver design," *IEEE Wirel. Commun.*, vol. 27, no. 2, pp. 180–187, 2020.
- [31] N. Yu, P. Genevet, M. A. Kats, F. Aieta, J.-P. Tetienne, F. Capasso, and Z. Gaburro, "Light propagation with phase discontinuities: generalized laws of reflection and refraction," science, vol. 334, no. 6054, pp. 333–337, 2011.
- [32] Ö. Özdogan, E. Björnson, and E. G. Larsson, "Intelligent reflecting surfaces: Physics, propagation, and pathloss modeling," *IEEE Wirel. Commun. Let.*, vol. 9, no. 5, pp. 581–585, 2019.
- [33] A. Abrardo, D. Dardari, and M. Di Renzo, "Intelligent reflecting surfaces: Sum-rate optimization based on statistical position information," *IEEE Trans. Commun.*, vol. 69, no. 10, pp. 7121–7136, 2021.
- [34] M. Najafi, V. Jamali, R. Schober, and H. V. Poor, "Physics-based modeling and scalable optimization of Large Intelligent Reflecting Surfaces," *IEEE Trans. Commun.*, vol. 69, no. 4, pp. 2673–2691, 2020.
- [35] W. Tang, M. Z. Chen, X. Chen, J. Y. Dai, Y. Han, M. Di Renzo, Y. Zeng, S. Jin, Q. Cheng, and T. J. Cui, "Wireless communications with reconfigurable intelligent surface: Path loss modeling and experimental measurement," *IEEE Trans. Wirel. Commun.*, vol. 20, no. 1, pp. 421–439, 2020.
- [36] Y. Li, J. Eisenbeis, X. Wan, S. Bettinga, X. Long, M. B. Alabd, J. Kowalewski, T. J. Cui, and T. Zwick, "A Programmable Metasurface Based TDMA Fast Beam Switching Communication System at 28 GHz," *IEEE Ant. Wirel. Propag. Let.*, 2021.
- [37] M. R. M. Hashemi, S.-H. Yang, T. Wang, N. Sepúlveda, and M. Jarrahi, "Electronically-controlled beam-steering through vanadium dioxide metasurfaces," Sci. Rep., vol. 6, no. 1, pp. 1–8, 2016.
- [38] Y. Zhou, X. Chen, C. Ko, Z. Yang, C. Mouli, and S. Ramanathan, "Voltage-triggered ultrafast phase transition in vanadium dioxide switches," *IEEE Elect. Dev. Let.*, vol. 34, no. 2, pp. 220–222, 2013.
- [39] J. Leroy, A. Crunteanu, A. Bessaudou, F. Cosset, C. Champeaux, and J.-C. Orlianges, "High-speed metal-insulator transition in vanadium dioxide films induced by an electrical pulsed voltage

over nano-gap electrodes," App. Phy. Let., vol. 100, no. 21, p. 213507, 2012.